Surface properties and electronic structure of low-index stoichiometric anatase TiO_2 surfaces

2010 J. Phys.: Condens. Matter 22 175008

(http://iopscience.iop.org/0953-8984/22/17/175008)

J. Phys.: Condens. Matter **22** (2010) 175008 (18pp) doi:10.1088/0953-8984/22/17/175008

Surface properties and electronic structure of low-index stoichiometric anatase TiO_2 surfaces

Zongyan Zhao[1,2], **Zhaosheng Li**[1,2,3,4] **and Zhigang Zou**[1,2,4]

[1] Ecomaterials and Renewable Energy Research Center (ERERC), Department of Physics, Nanjing University, Nanjing 210093, People's Republic of China
[2] National Laboratory of Solid State Microstructures, Nanjing University, Nanjing 210093, People's Republic of China
[3] Department of Materials Science and Engineering, Nanjing University, Nanjing 210093, People's Republic of China

E-mail: zsli@nju.edu.cn and zgzou@nju.edu.cn

Received 15 January 2010, in final form 4 March 2010
Published 12 April 2010
Online at stacks.iop.org/JPhysCM/22/175008

Abstract
Using the ultrasoft pseudopotential plane wave method, we present a systematic theoretical study of six low-index stoichiometric anatase TiO_2 surfaces, including (101), (100), (001), $(103)_f$, $(103)_s$ and (110) surfaces. We paid particular attention to their surface properties and electronic structure, including the surface band structure, layer-resolved density of states, surface electron distribution and electrostatic potential. After surface relaxation, the electrons in the dangling bond of surface atoms redistributed inwards, and the surface states changed correspondingly. So the surface energy was reduced and then stabilized. Based on these calculated results, one can better understand the selective activities of different anatase TiO_2 surfaces, and some relevant phenomena of TiO_2 nanoparticles.

(Some figures in this article are in colour only in the electronic version)

1. Introduction

Nowadays, energy depletion and ecological environment deterioration are two severe issues which urgently need to be solved. Among the many solutions, heterogeneous photocatalysis technology, which is based on oxide semiconductor theory, is the most potentially promising. Titanium dioxide (TiO_2), as a prototype for photocatalytic materials, has been extensively investigated in recent years [1–5]. Because of its unique physical and chemical properties, TiO_2 is also widely used in other fields, such as pigments, coatings, electronic devices, implants, gas sensors, and photovoltaic conversion [4, 6]. Furthermore, in the field of surface science, TiO_2 also acts as a prototype for metal oxide surfaces. Many excellent performances of TiO_2 are directly related to its surface properties, because almost all of the physical and chemical reactions usually occur on its surface. Therefore, in-depth investigation of the surface properties of TiO_2 is very important and will help in understanding and improving the relevant applications of TiO_2 [4]. Diebold has published excellent reviews that have provided a comprehensive overview of studies on the main low-index surfaces of TiO_2 [7–9].

In recent decades, both experimental and theoretical research has already paid attention to the surface properties of TiO_2. The experimental technologies of surface analysis, including scanning tunneling microscopy (STM), x-ray photoelectron spectroscopy (XPS), Auger electron spectrometry (AES), electron energy-loss spectroscopy (EELS), atomic force microscopy (AFM), low energy electron diffraction (LEED), etc, are the most effective means to provide surface information on materials. However, to provide further detailed information is still beyond their capability, especially for surface electronic structure [10]. At the atomic-scale level, reliable theoretical calculations can complement this deficiency of experimental technologies, and are becoming increasingly indispensable in the field of surface science. As a typical example, Kubo *et al* integrated experimental measurements with density functional calculations to elucidate the nature of the surface reconstructions of rutile TiO_2 surfaces [11].

[4] Authors to whom any correspondence should be addressed.

In recent years, for the surface of TiO_2, most theoretical studies have focused on the rutile (110) surface, because this surface is easily prepared and has accumulated a wealth of experimental data. Vogtenhuber *et al* [12] calculated the electronic structure and geometry of a clean rutile TiO_2 (110) surface. They obtained a work function of 6.79 eV that matched with the experimental result of 6.83 eV, and some surface states to explain the photoemission experimental phenomenon. Other research groups calculated relaxed and/or reconstructed rutile TiO_2 surfaces [11, 13–20]. They found that the (110) surface is the most stable, and proposed some possible models for non-stoichiometric surfaces. Although anatase is the metastable phase for TiO_2, it has already shown remarkable photocatalytic performance. Also, it is the preferred structure for TiO_2 nanoparticles. But relevant research on anatase TiO_2 surfaces is lacking compared with rutile. There are two possible reasons: it is very difficult to prepare a sufficiently large and pure single anatase crystal; and the anatase structure is more complicated than rutile structure. It was not until 2000 that Hebenstreit *et al* [21] reported for the first time a STM study of a single-crystalline anatase TiO_2 (101) surface. They found there is no reconstruction phenomenon and that less surface defects made this surface more stable. Next, Hengerer *et al* [22] studied the well-defined anatase TiO_2 (101) and (001) surfaces by secondary electron imaging (SEI) and LEED. Selloni's group systematically researched various surfaces for anatase TiO_2 [23–25]. Their calculation included surface energy, surface relaxation, and surface morphology. According to Wulff construction theory, they determined the equilibrium crystal shape of anatase, which closely resembles the shape of naturally occurring anatase mineral specimens.

As a matter of fact, for both rutile surfaces and anatase surfaces, most of the previous calculations discussed surface atomic structure and surface energy, and only a few workers reported their surface electronic structures [26–28]. Obtaining knowledge about the surface electronic structure of materials is fundamental to analyzing all surface physical and chemical phenomena. In particular for photocatalysis, the surface electronic properties are very important, because the essence of photocatalysis is the movement of photo-induced carriers. The process of photocatalysis includes the following steps: photon excitement, carrier movement, electron–hole recombination, and carrier transfer between the photocatalyst's surfaces and the reactants. In these steps, the last step is the most critical and is directly related to the surface properties of photocatalyst [29]. However, the existing literature does not provide sufficient information about this aspect, so this process is still not adequately understood. In order to attempt to resolve this issue, we adopted the ultrasoft pseudopotential plane wave method based on the density functional theory (DFT) framework to investigate systematically low-index stoichiometric anatase TiO_2 surfaces, including (101), (100), (001), (103) and (110) surfaces. The emphasis of the present work is placed on surface electronic structure, and the relationship between surface relaxation and surface electronic structure. All of the surfaces were calculated by the same computation protocols, which is an advantage in making a straightforward comparison between different surfaces.

This paper is organized as follows. Computational methods and models are described in section 2. In section 3.1, a short overview of the surface structure and surface properties of all the surfaces is presented. The surface electronic structures are discussed in the remaining part of section 3. Finally, we will summarize the calculation results and draw some conclusions in section 4.

2. Computational methods

All of the DFT calculations in the present work have been performed with the Cambridge Serial Total Energy Package (CASTEP) code [30]. The ultrasoft pseudopotential was chosen in the calculations, because it has several advantages, both in efficiency and velocity. The Kohn–Sham wavefunctions of the valence electrons were expanded using a plane wave basis set within a specified energy cutoff that was chosen as 380 eV. Exchange and correlation effects were described by the Perdew–Burke–Ernzerhof (PBE) generalized gradient approximation [31]. The Monkhorst–Pack scheme K-points grid sampling was set as $7 \times 7 \times 1$ (or $5 \times 3 \times 1$, different surface has different setting in this region) for the irreducible Brillouin zone. A $30 \times 30 \times 432$ (or $40 \times 72 \times 300$, different surface has different setting in this region) mesh was used for fast Fourier transformation. The minimization algorithm chosen was the Broyden–Fletcher–Goldfarb–Shanno (BFGS) scheme [32]. In order to get accurate results, we optimized the atomic coordinates, which were obtained by minimizing the total energy and atomic forces. This was done by performing an iterative process in which the coordinates of the atoms are adjusted so that the total energy of the structure is minimized. By doing so, we could obtain stable structures for all the models. The relaxation run was considered to have converged when the force on the atomic nuclei was less than 0.01 eV $Å^{-1}$, the stress on the atomic nuclei was less than 0.02 GPa, the displacement of the nuclei was less than 5×10^{-4} Å, and the energy change per atom was less than 5×10^{-6} eV. Then we calculated the surface properties and the electronic structures of the optimized surface models.

By these methods, we firstly optimized the bulk anatase TiO_2 supercell, and got the bulk lattice parameters as follows: $a = b = 3.7748$ Å, $c = 9.5990$ Å, $d_{ap} = 1.9883$ Å, $d_{eq} = 1.9318$ Å, $2\theta = 155.403°$. They were in good agreement with experimental values [33]: $a = b = 3.7848$ Å, $c = 9.5124$ Å, $d_{ap} = 1.9799$ Å, $d_{eq} = 1.9338$ Å, $2\theta = 156.230°$. Our calculation gave a bulk band gap of 2.13 eV, coinciding with other theoretical calculations [23, 34]. These results implied that our calculation methods are reasonable, and the calculated results should be authentic.

In order to describe the surfaces, we used the slab supercell method. All the surfaces were modeled using slabs of up to 16 tri-layers (O–Ti–O) of TiO_2. A vacuum space of 20 Å has been used to separate the slab from its periodic image along the surface normal direction. For all the geometry optimizations presented below, the central four tri-layers of the slab were kept fixed at the bulk positions and the six outermost tri-layers of atoms on both sides of the slab were relaxed by the method mentioned above. For each surface, there are

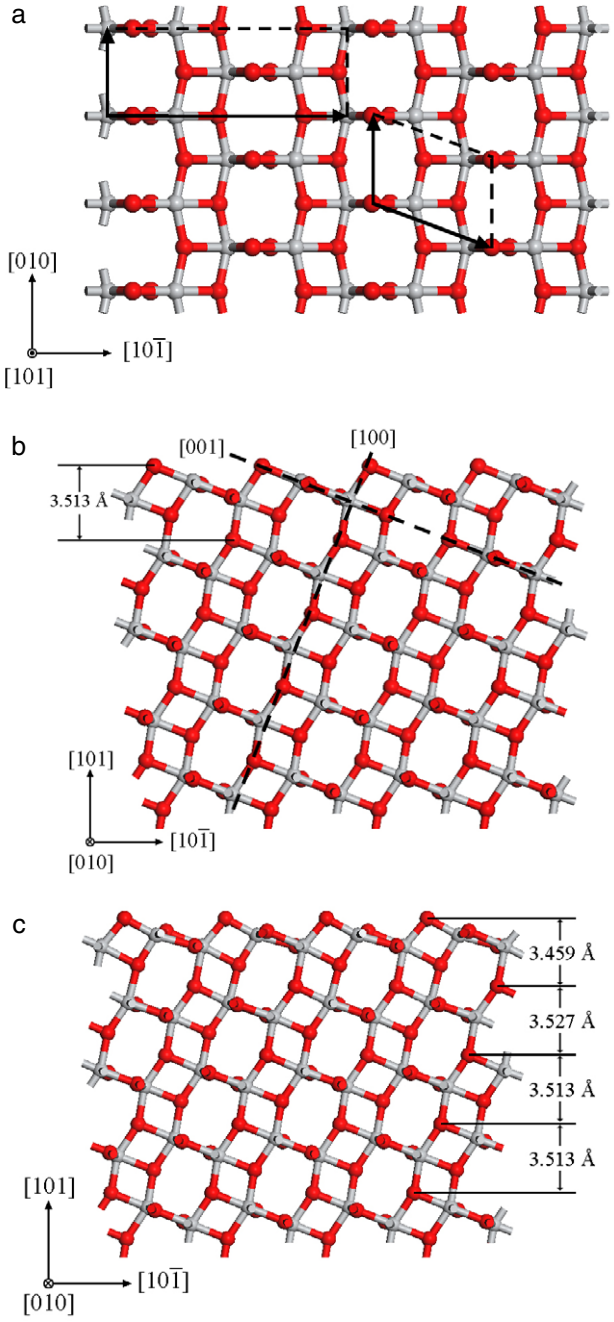

Figure 1. Schematic top view (a) and side view ((b): before the relaxation; (c): after the relaxation) of the TiO_2 (101) surface. The Ti and O atoms are denoted by gray and red spheres, respectively. The primitive and conventional cells are also shown in (a), and the corresponding lattice parameters are displayed in table 1. Only 10 tri-layers are shown in (b) and (c).

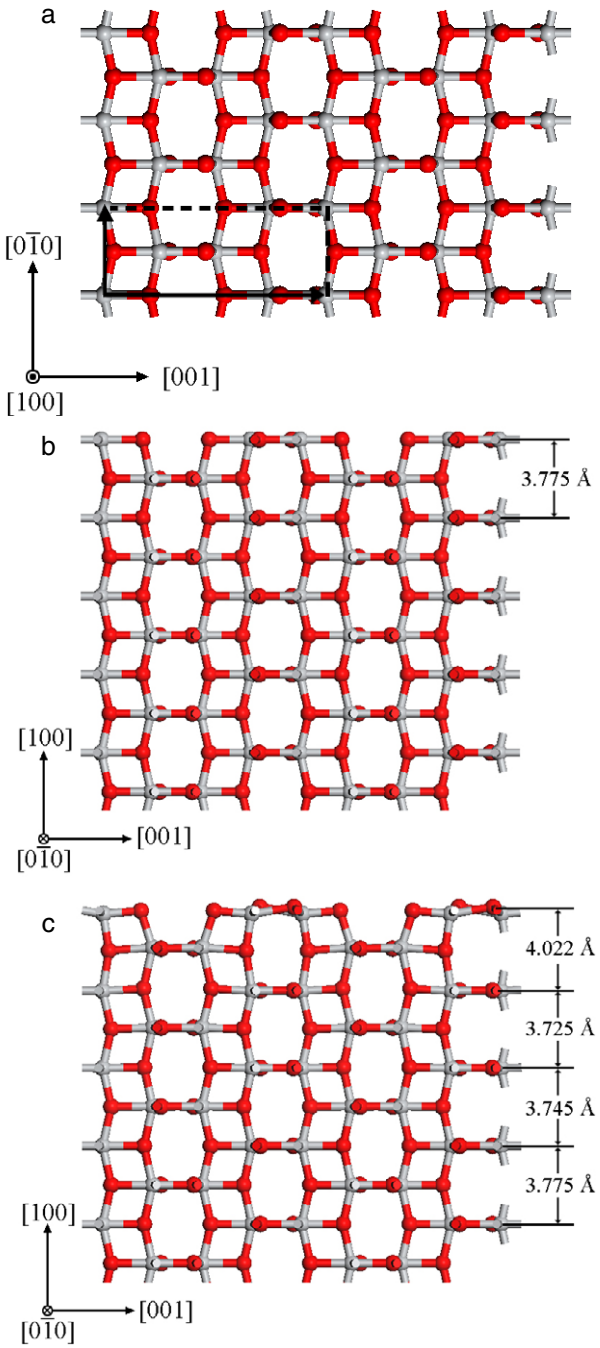

Figure 2. The same as figure 1 but for the (100) surface.

different possible terminations surfaces. We firstly calculated every possible terminated surface, and then determined the most stable surface by the energy minimum principle. In order to conveniently discuss and compare different surfaces, we adopted the p-rectangular Bravais lattice that has *pm* space group symmetry [35]. The band structure for all surfaces were calculated along the high symmetry lines Γ–J–K–J′–Γ of the surface Brillouin zone (SBZ). The work function was calculated as the difference between the average electrostatic potential in the vacuum and the Fermi energy of the slab. Finally, using the Helmholtz equation, we calculated the change of surface dipole moment based on the work function [36].

3. Results and discussions

3.1. Surface properties

For each surface, by analyzing the surface energy of all possible terminated planes, we obtained the stable unrelaxed surface, as shown in figures 1–6. Two different terminated planes for the (103) surface (a 'faceted' and a 'smooth'

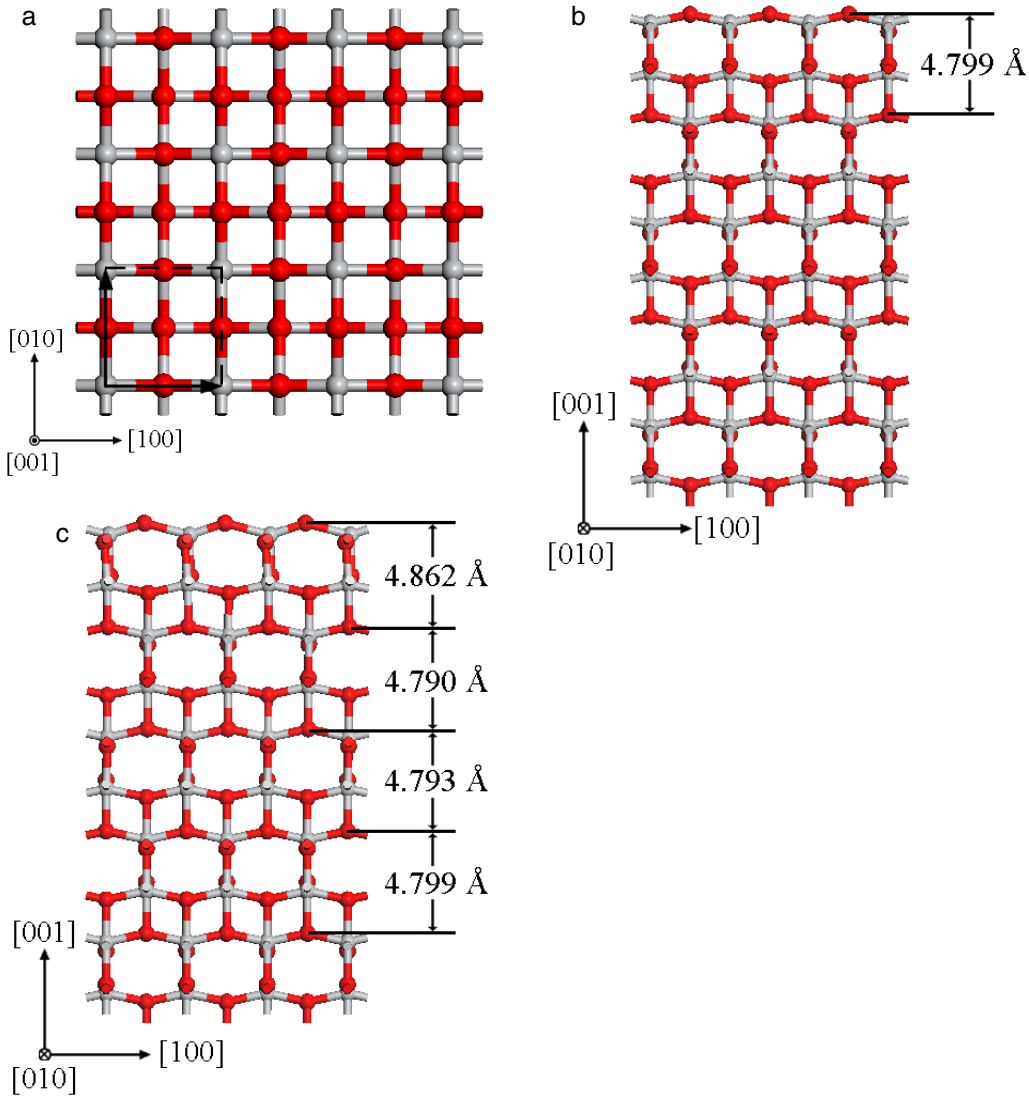

Figure 3. The same as figure 1 but for the (001) surface.

one) have been considered. According to Tasker's category, based on electrostatic considerations [37], (100)/(110) surfaces belong to type 1 surfaces (neutral planes with equal numbers of anions and cations parallel to the surface); (001)/(101)/(103) surfaces belong to type 2 surfaces (charged planes but no dipole moment perpendicular to the surface). That is to say all of the surface models in the present work are stable. Also, according to the rules of autocompensation [38], one could draw the same conclusion, because the excess charge from cation-derived dangling bonds compensates anion-derived dangling bonds. In table 1, the surface energies before and after surface relaxation are given. Although there are certain differences between our results and other calculated results in the literature, the surface energy order is completely consistent with the previous literature results. This difference maybe relate to having more atomic layers in our models and different calculation methods [28]. The surface energies of $(101)/(100)/(103)_f$ unrelaxed surfaces are larger than that of the (001) unrelaxed surface, but this sequence is reversed in the relaxed surfaces. By comparing these energies, we found that: the $(103)_s/(110)$ surface release more energy to relax; surface relaxation is not obvious in (001) surface; the two terminated surfaces of (103) have a very close surface energy after surface relaxation.

The work function is caused by two parts: a direct result of the cut-off of the lattice period, and the charge redistribution effect. The first part is reflected in the work function of the unrelaxed surfaces. While the surface is relaxing, the charge will be redistributed, and the surface dipole moment will accordingly change. The change of work function reflects this surface effect. Thus we could obtain the change of surface dipole moment from the change of surface work function. The work function expresses the difficulty of losing an electron from a surface; on the other hand, the electron affinity energy expresses the ability of getting an electron from the adsorbate. Together they reflect the redox ability of different surfaces [39]. Based on these data, one can understand the selective reactivity for various anatase TiO_2 surfaces. In table 1, we also showed these changes before and after surface relaxation, and more relevant discussions will be given in below text.

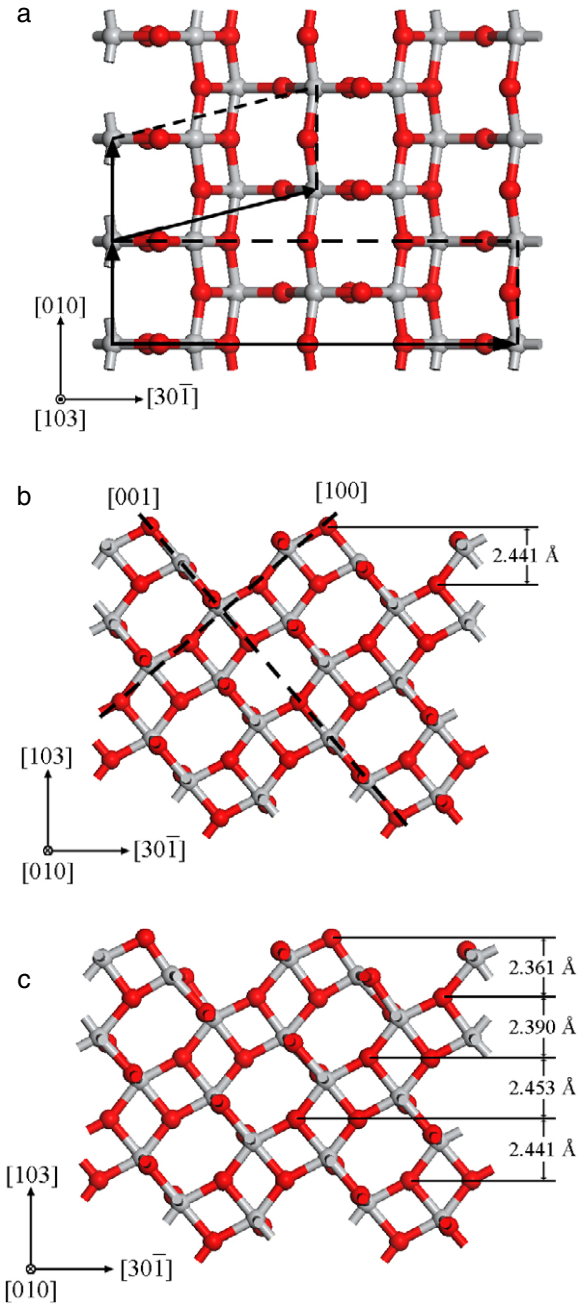

Figure 4. The same as figure 1 but for the $(103)_f$ surface.

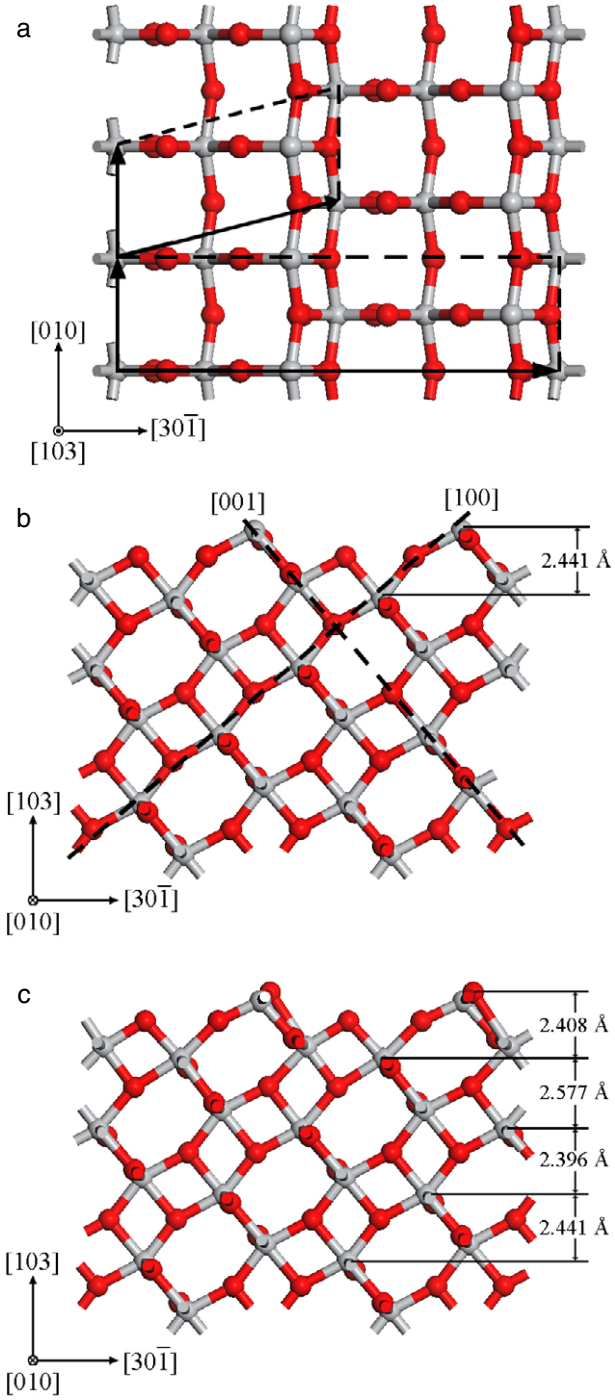

Figure 5. The same as figure 1 but for the $(103)_s$ surface.

In the present work, all of the atom displacements and the changes of bond length are in agreement with Selloni's [23] and Labat's [28] calculated results. Therefore, we will not repeat these results in this paper.

3.1.1. (101) surface. For anatase TiO_2, the (101) surface is the thermodynamically most stable surface [7, 23, 28]. Most literature, both experimental and theoretical, has focused on this surface. From figure 1(b), it has sawtooth profile along the [10$\bar{1}$] direction, which can be seen as a small step surface or a vicinal surface constructed by the (100) and (001) surfaces. One of the prominent results is that the third atomic layer of 3c-O atom (threefold-coordinated O atom, similarly hereinafter) rises above the second atomic layer of 5c-Ti after surface relaxation. According to Tasker's category, the (101) surface changes to a polar surface from a non-polar surface, and has a certain surface dipole moment, as shown in table 1. This surface effect will significantly influence the anatase TiO_2 performance. Each periodic plane has two tri-layers (O–Ti–O–O–Ti–O) in this surface, and we denote the distance between any two adjacent planes in figure 1(c). Surface relaxation occurs on the outermost two planes, and no surface reconstruction can be observed for this surface; this is in line

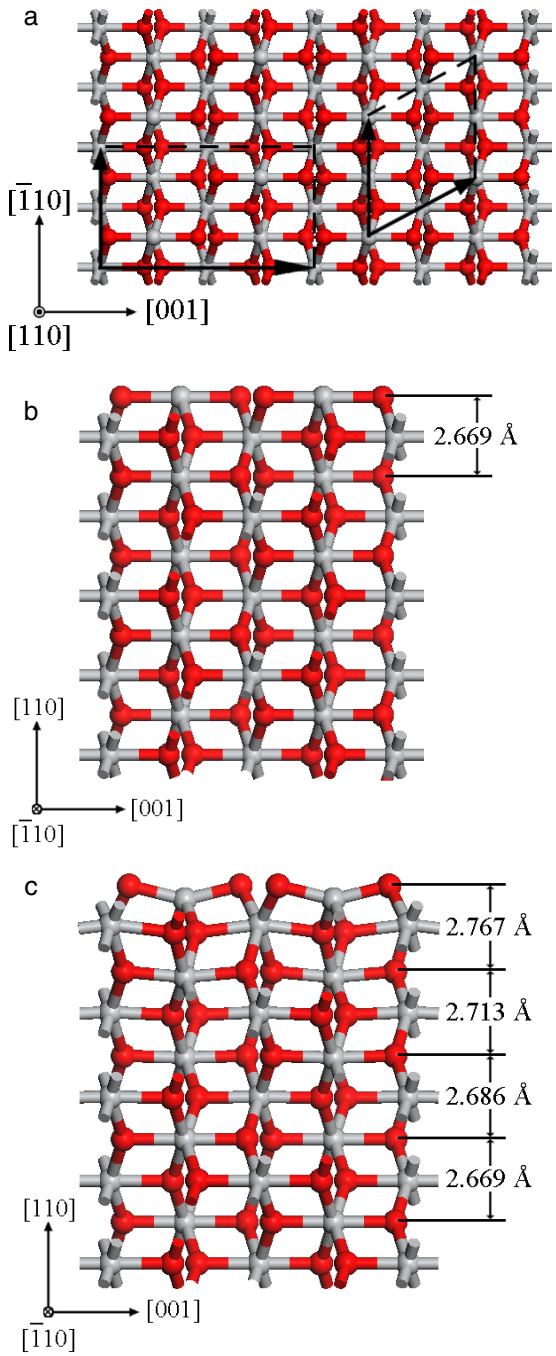

Figure 6. The same as figure 1 but for the (110) surface.

with the experimental results [21, 22, 40]. In each plane, the distance between Ti atoms and the thickness decrease.

3.1.2. (100) surface. For water or other small molecules, the preferred adsorption formation is dissociative adsorption on the anatase (100) surface [41–43]. The production of hydroxyl radicals is very crucial for the photocatalytic performance of TiO_2. Also, the surface properties of anatase TiO_2(100) surface are of great importance in chemical technology, because it is best suited as a support for oxide catalysts [44, 45]. Before surface relaxation, each periodic plane is a stoichiometric and non-polar surface. The surface structure in the present work is in good agreement with the LEED pattern [46]. There are two types of oxygen atoms in the plane: one is in a Ti–O bond parallel to the plane; and the other is in a Ti–O perpendicular to the plane. After surface relaxation, in the first plane, 3c-O clearly relaxes outward, while 2c-O slightly relaxes outward and 5c-Ti clearly relaxes inward. So this relaxed surface is an oxygen-rich and polar surface just like the (101) surface. From the surface down, the odd Ti atomic layers relax inward, and the even Ti atomic layers relax outward. Surface relaxation occurs on the outermost four planes, as shown in figure 2(c), and in the present work we did not consider the surface reconstruction.

3.1.3. (001) surface. The minority (001) surface exhibits a very high reactivity, and plays a crucial role for nanoparticles [39, 47–49]. Furthermore, it enhances catalytic activity for industrially supported catalysts [50, 51]. Recently, researchers have reported that it could be synthesized by different chemical methods [39, 48, 52]. Each periodic plane contains a tri-layer (O–Ti–O). In surface relaxation, this surface keeps the non-polar character, and the relaxation occurs at the outermost four tri-layers. The LEED and STM measurements also found no reconstructive surface [53, 54]. In the [001] and [010] direction, the atomic displacement is very small. But in the [100] direction the oxygen atomic displacements are much larger: the oxygen atoms in the first tri-layer displace along the [$\bar{1}$00] direction, while those in the second tri-layer displace along the [100] direction. So on the relaxed surface, the bonds between 2c-O and its two nearest neighboring 5c-Ti are not equivalent, and the mirror plane symmetry along the [100] is broken.

3.1.4. (103) surfaces. As Selloni *et al* had discussed two possible terminated planes (faceted surface: $(103)_f$; and smooth surface: $(103)_s$), this present work also discussed these two surfaces. High-resolution TEM images indicated the (103) surface can be exposed depending on the processing conditions for the anatase nanoparticles [55], and Herman *et al* have determined that the anatase TiO_2 (001) (1×4) surface reconstructs to form a microfaceted surface that exposes (103) and ($\bar{1}$03) planes, thus they surmised that the (103) surface of anatase is lower in energy than the (001) [54]. In our calculations, the surface energy of $(103)_f$ is slightly lower than that of (001), which verifies this surmise. The profile of the (103) surface is similar to the (101) surface: the $(103)_f$ surface is a large step surface, and the $(103)_s$ is more complex. In the $(103)_f$ surface, the periodic plane contains two tri-layers (O–O–Ti–Ti–O–O); and in $(103)_s$, the periodic plane also contains two tri-layers (Ti–O–O–O–O–Ti). In the $(103)_s$ surface, the second atomic layer 3c-O rises above the first atomic layer 5c-Ti, so the surface becomes a polar surface and has large surface polar moment, as shown in table 1. For both the possible terminated planes, the surface relaxation obviously occurs in the outmost six tri-layers.

Table 1. Two-dimensional lattice parameters, formation energies and work functions of various anatase TiO_2 surfaces in the present work. The surface dipole moments were calculated from the difference of work function before and after surface relaxation (see the text). The indications of primitive cell and conventional cell are seen in figures 1–6.

	2D lattice parameter		Surface energy (γ) (J m^{-2})		
	Primitive cell	Conventional cell	Unrelaxed	Relaxed	Difference
(101)	$a = 5.492$ Å, $b = 3.775$ Å $\gamma = 110.101°$	$a = 10.315$ Å, $b = 3.775$ Å $\gamma = 90°$	1.297	0.609	0.688
(100)	$a = 3.775$ Å, $b = 9.599$ Å $\gamma = 90°$	$a = 3.775$ Å, $b = 9.599$ Å $\gamma = 90°$	1.623	0.712	0.911
(001)	$a = b = 3.775$ Å $\gamma = 90°$	$a = b = 3.775$ Å $\gamma = 90°$	1.228	1.082	0.146
$(103)_f$	$a = 7.659$ Å, $b = 3.775$ Å $\gamma = 75.733°$	$a = 14.845$ Å, $b = 3.775$ Å $\gamma = 90°$	1.582	1.052	0.530
$(103)_s$	$a = 7.659$ Å, $b = 3.775$ Å $\gamma = 75.733°$	$a = 14.845$ Å, $b = 3.775$ Å $\gamma = 90°$	2.455	1.136	1.319
(110)	$a = 5.338$ Å, $b = 5.492$ Å $\gamma = 60.920°$	$a = 5.338$ Å, $b = 9.599$ Å $\gamma = 90°$	2.237	1.234	1.003

	Work function (Φ) (eV)		Electron affinity energy (χ) (eV)		Change of surface dipole moment ($\Delta\mu$) (Debye)
	Unrelaxed	Relaxed	Unrelaxed	Relaxed	
(101)	5.981	6.578	4.052	4.384	1.033
(100)	4.289	5.010	2.843	2.807	0.693
(001)	4.501	4.924	2.982	3.193	0.160
$(103)_f$	6.093	6.341	4.836	4.450	0.269
$(103)_s$	2.750	4.988	1.701	2.737	3.327
(110)	3.497	4.599	1.984	2.393	1.498

3.1.5. (110) surface. Compared with other low-index surfaces, the (110) surface is rarely considered. Noble metals, such as Au and Ag, can be loaded and perfectly accommodated on the anatase (110) surface, resulting in the surprising catalytic properties [56, 57]. Before surface relaxation, each periodic plane is a stoichiometric and non-polar surface. The first plane contains two 4c-Ti and four 2c-O. In Selloni's paper, they found that oxygen atoms in the first plane display different displacements from the equilibrium positions, and are no longer equivalent. However, in the present work, we found that, even in the relaxed surface, these oxygen atoms still display equivalent properties owing to the same coordinated circumstance and surface symmetry. From the surface down, the atomic displacements in odd planes is opposite to the even planes: in odd planes, the titanium atoms displace downward, and oxygen atoms displace upward; while in even planes, titanium atoms displace upward, and oxygen atoms displace downward. Therefore, the dipole moment remains zero along the [110] direction. After surface relaxation, the crystal plane spacing expands, and the surface relaxation obviously occurs in the outermost four planes.

3.2. The electronic structure (part I)

The calculated energy band structures of all surfaces are plotted in figures 7–12. In order to identify the surface states, the corresponding layer-resolved local density of states (DOS) are also displayed. By analyzing the amplitude and bonding ways of the layers, we could determine the surface states that are localized in different layers and different atoms. The identified surface states are indicated by dash and/or dotted lines. We do not show the surface states when they appear as resonances inside the projected bulk bands. The common features to all surfaces are as follows.

(i) Overall, there is a clear fundamental band gap between the valence band (VB) and the conduction band (CB). For every unrelaxed surface, the octahedral crystal field effect and the surface effect, the phenomenon by which the CB is divided into two parts, is more obvious than that of the bulk phase, forming an obvious stomach gap.

(ii) Because of the dangling bonds of 2c-O and 5c-Ti at the outmost layer, there are some surface states in the fundamental band gap whose positions are very close to the VB top or CB bottom. These surface states arise from occupied 2p states of 2c-O and unoccupied 3d states of 5c-Ti, respectively. A separate surface state could be found in the deep energy level region, which arises from occupied 2s states of 2c-O. After surface relaxation, due to electron transfer, these dangling bonds are partially saturated, and thus the surface states in the band gap disappear. At the same time, the surface states of 5c-Ti fill the stomach gap with unoccupied 3d states.

(iii) The disappearance of surface states in the fundamental gap led to the increase of the surface band gap. After surface relaxation, the band width decreases, and the VB as a whole moves closely to the Fermi level, while the CB as a whole moves away from the Fermi level. The widths of electronic energy band and the distance from 2s state of 2c-O to the bulk projected states decrease. In this way, the surface energy can be reduced and become stable.

(iv) In addition to identification of the surface states, the local DOS map also shows that the surface states decay rapidly with the depth from the surface, i.e. they are concentrated

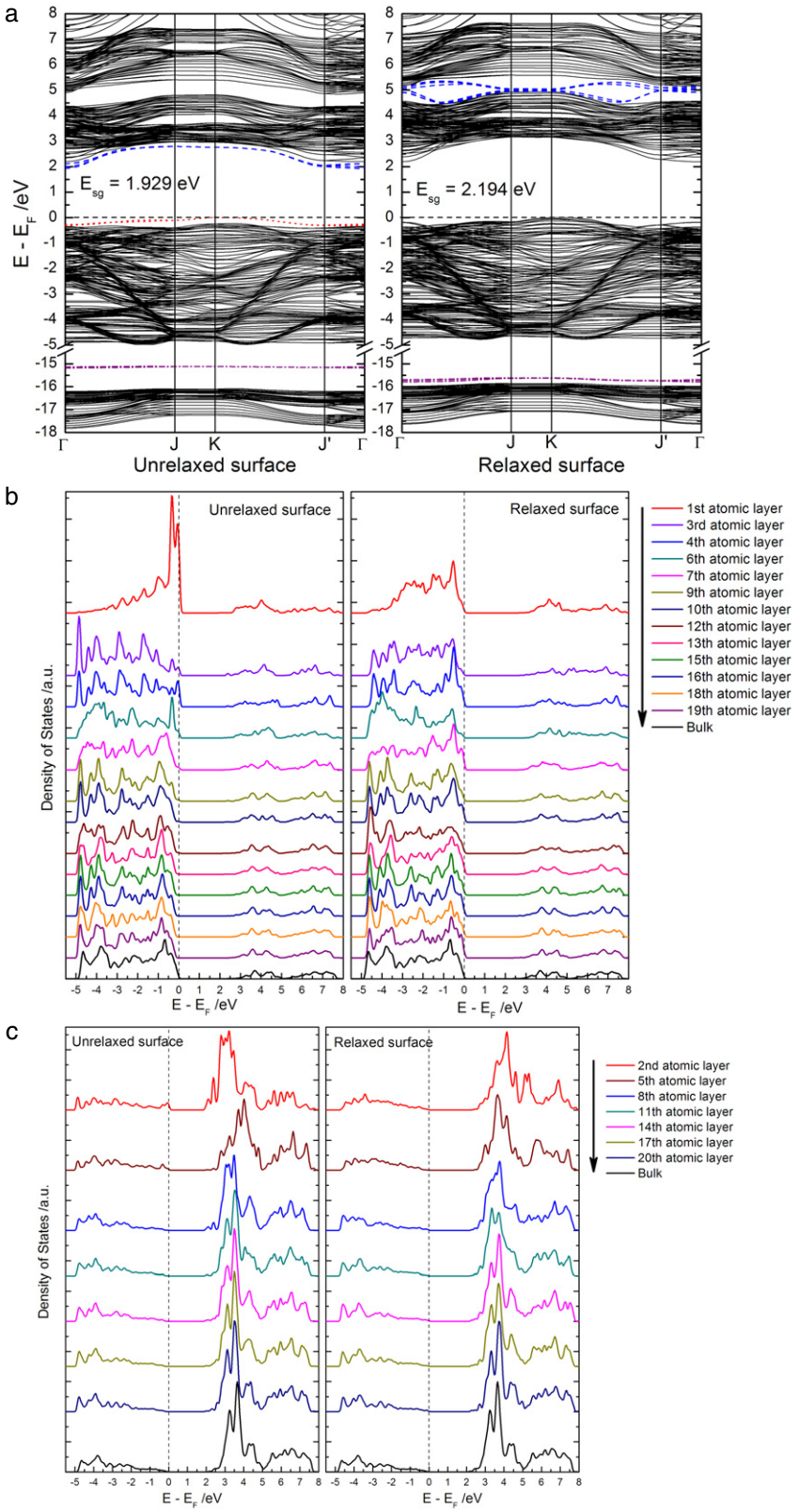

Figure 7. Electronic structure of the anatase TiO_2 (101) surface. (a) The surface band structure in SBZ before and after surface relaxation (red dotted line: O 2p state; blue dashed line: Ti 3d state; purple dash dot line: O 2s state; black dashed line: Fermi energy level), and the surface band gap is also given. The layer-resolved local partial DOS of the O 2p state (b) and Ti 3d state (c) before and after surface relaxation.

in the few outermost atomic layers. As the depth continues to increase, the DOS of each surface atom will become the same as that in the bulk phase.

(v) In the unrelaxed surfaces, the hybridization between surface atoms is very weak. After surface relaxation, these surface states change to extended states from localized

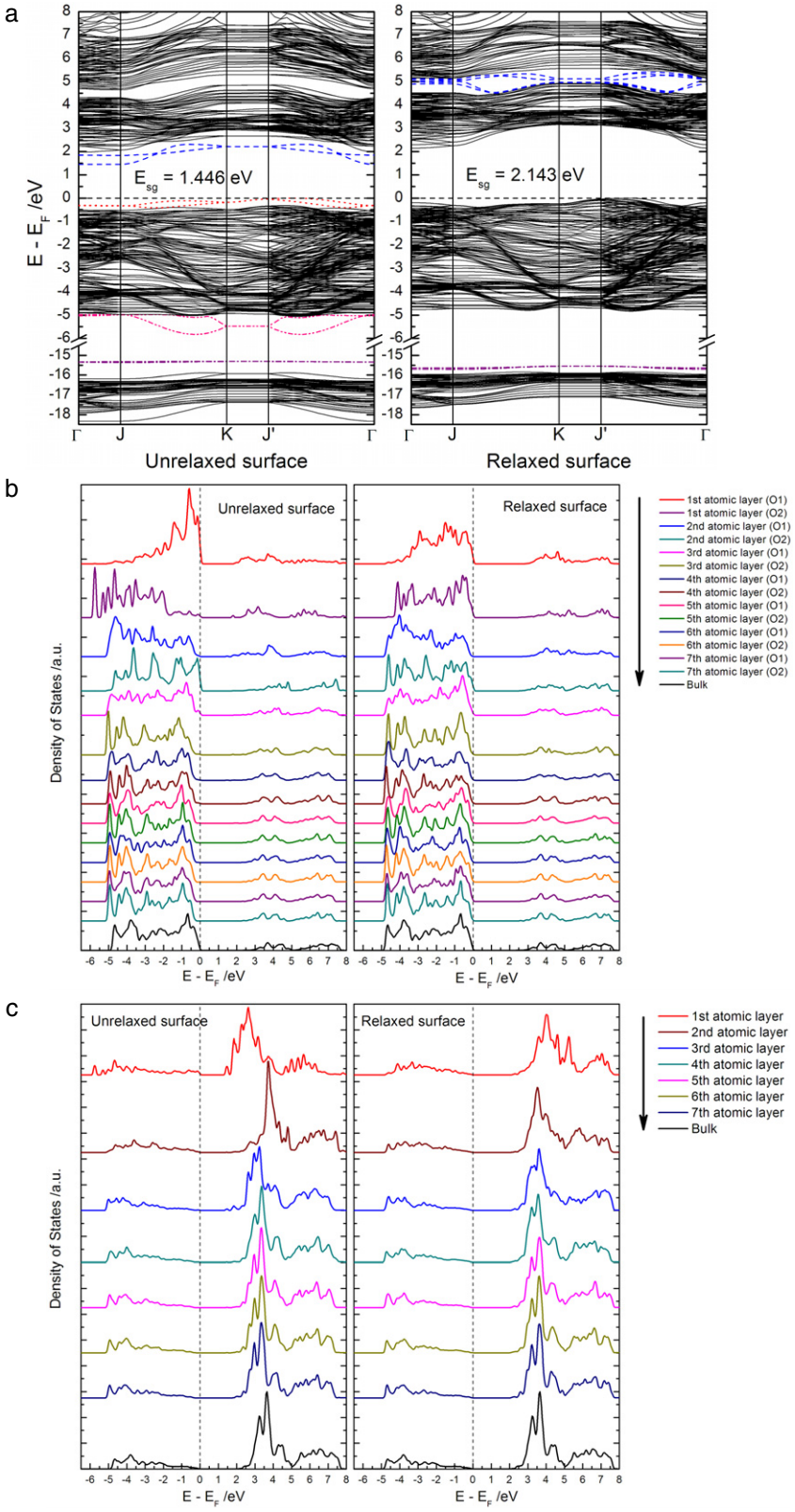

Figure 8. The same as figure 7 but for the (100) surface.

states, and the hybridization is enhanced by electron transfer.

Comparing figures 7–12, there are some differences in the electronic structure for different surfaces.

(i) In the (100) and $(103)_s$ unrelaxed surfaces, there are some surface states forming with 2p states of 3c-O in the first plane under the VB bottom, which disappear in the relaxed surface. In the (100) surface, each plane has

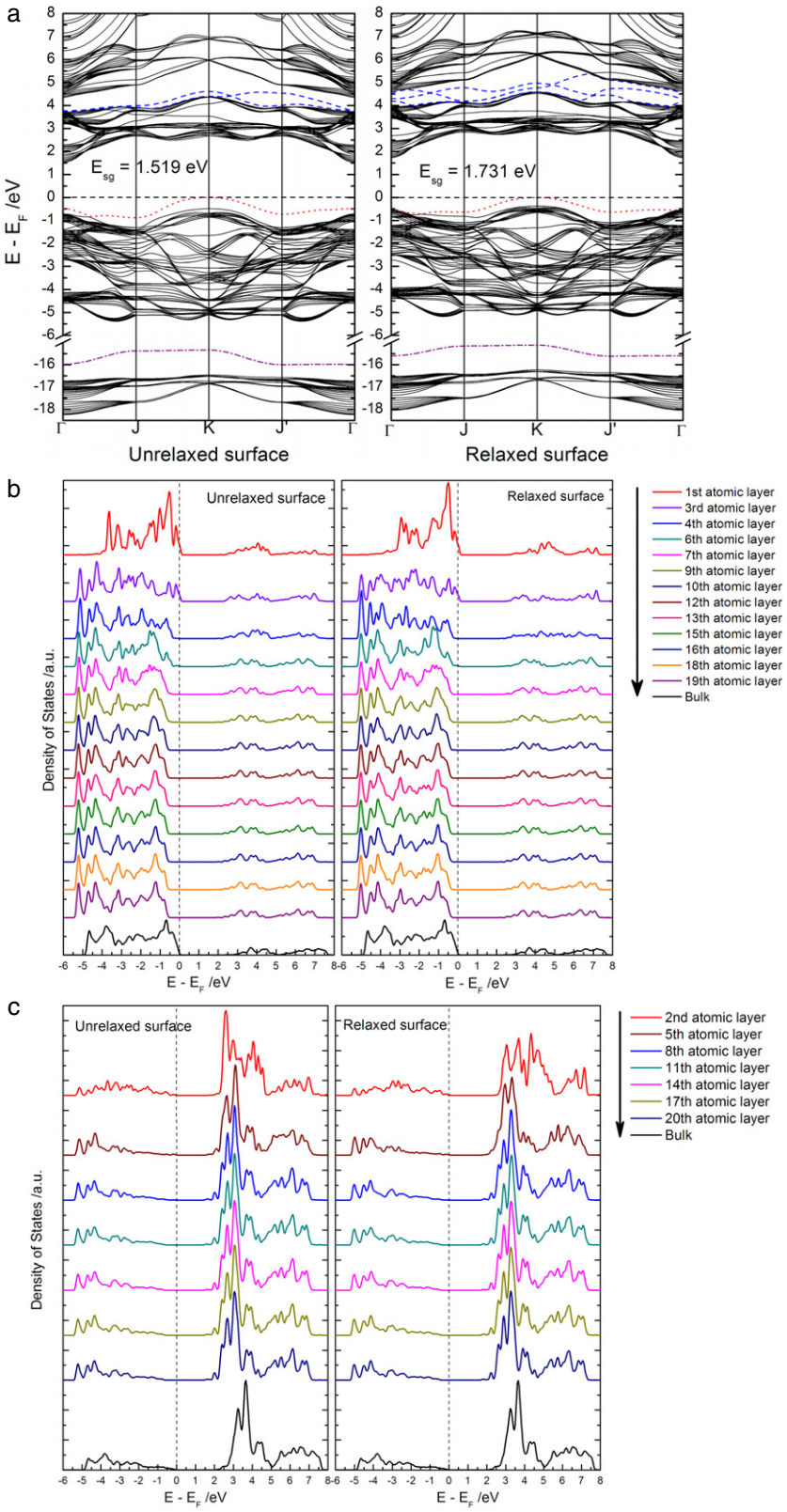

Figure 9. The same as figure 7 but for the (001) surface.

two nonequivalent oxygen atoms, so they have different surface states in the three outermost planes, as shown in figure 8.

(ii) For the (001) and $(103)_f$ surfaces, the relaxation is far less pronounced than for other surfaces. So the electronic structure undergoes less change after surface relaxation.

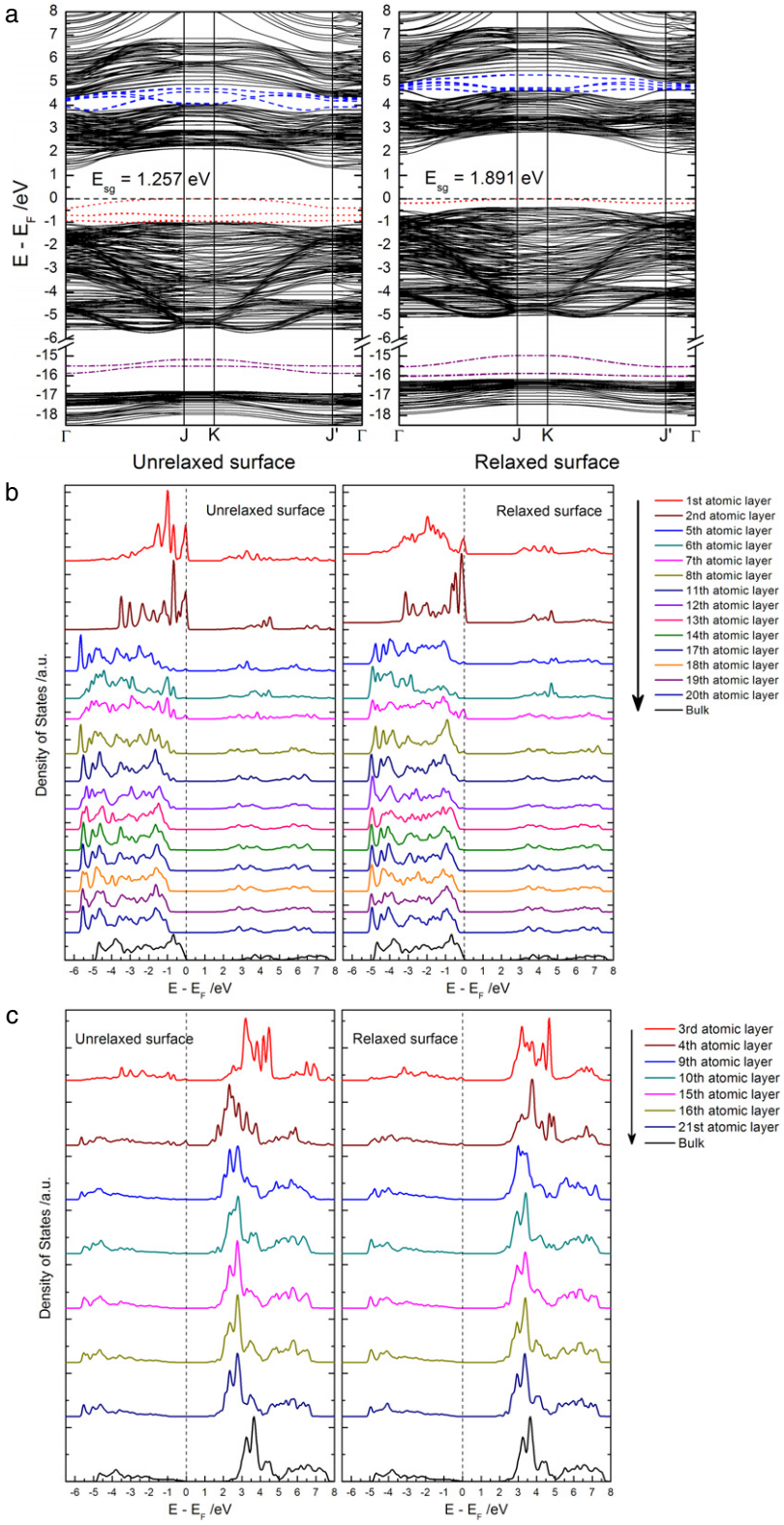

Figure 10. The same as figure 7 but for the $(103)_f$ surface.

Before surface relaxation, although the surface states of 5c-Ti concentrate at the bottom of the CB, it does not form an isolated state in the band gap. At the same time, the stomach gap is partially or completely filled, too. After surface relaxation, the isolated surface state above the top of VB does not disappear, and the stomach gap is completely filled.

(iii) For the (001) surface, with a higher symmetry than the other surfaces, the band structure has a high degree of degeneracy. In the CB, there are surface resonant states

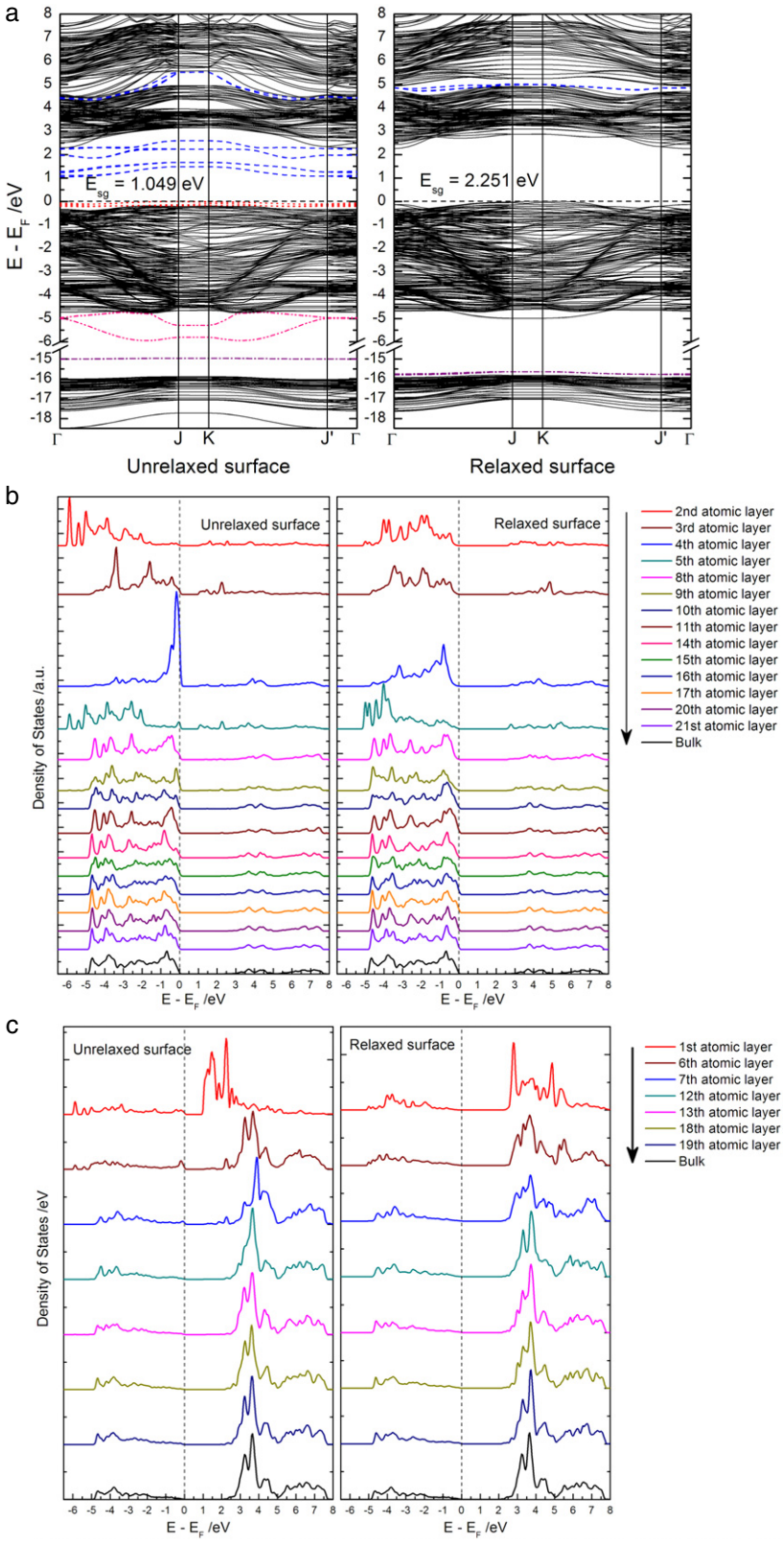

Figure 11. The same as figure 7 but for the $(103)_s$ surface.

arising from the 3d states of 5c-Ti. The surface relaxation only occurs in the outmost tri-layer.

(iv) For the (103) surface, there are more surface states due to more dangling bonds. In the first plane of the (103) surface, the electronic states of surface atoms are entirely different from each other, owing to the completely different coordinated environment compared with the bulk phase.

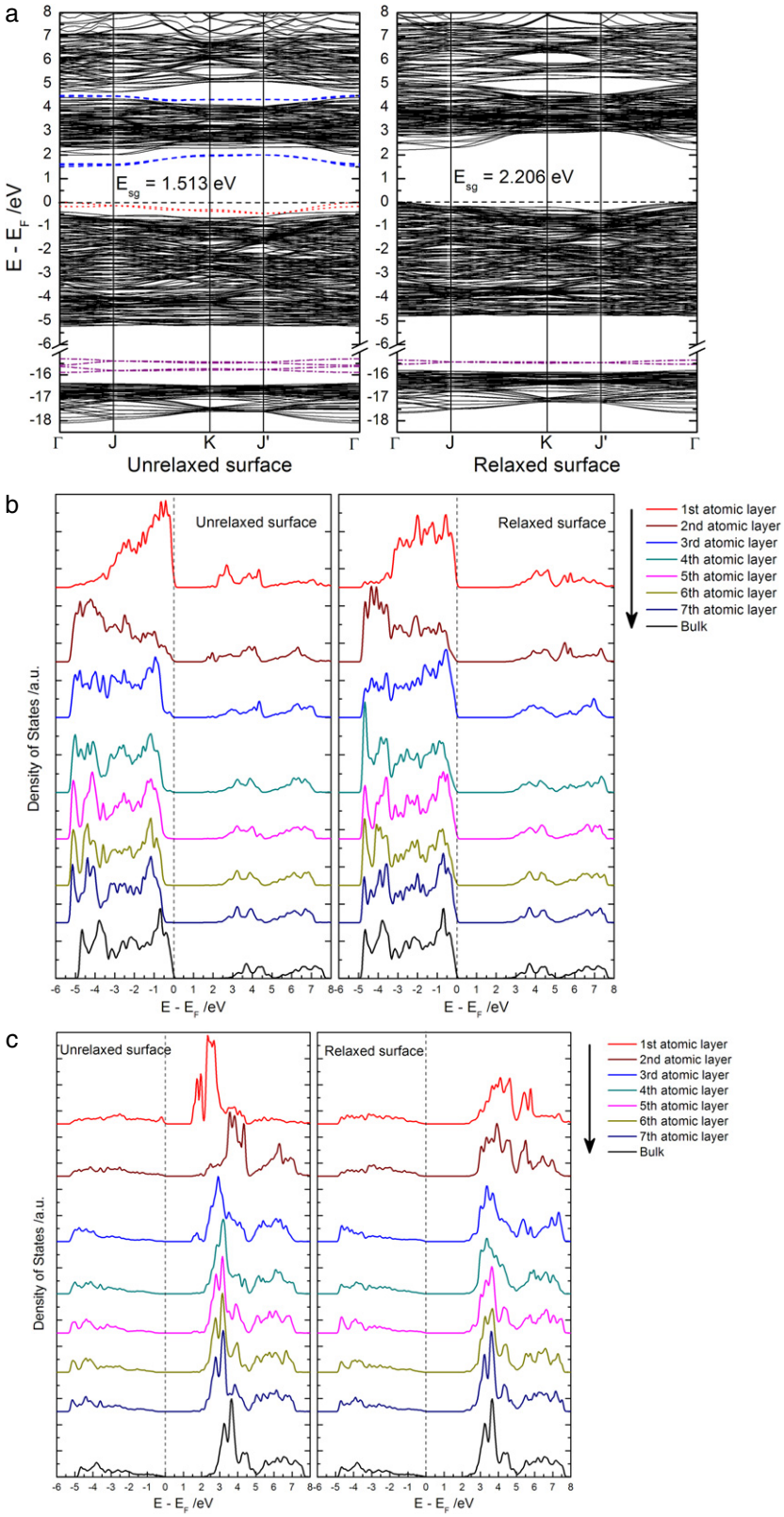

Figure 12. The same as figure 7 but for the (110) surface.

(v) For the (110) surface, the dispersion of the surface band structure is far weaker than that of the other surfaces.

(vi) The DFT underestimates the band gaps of semiconductors, so the absolute values of the calculated band gaps are not reliable [58]. But the relative values are reliable under the same calculation protocols. Because of the existence of surface states in the fundamental band gap, the calculated surface band gaps of the $(001)/(103)_f$ relaxed surface and

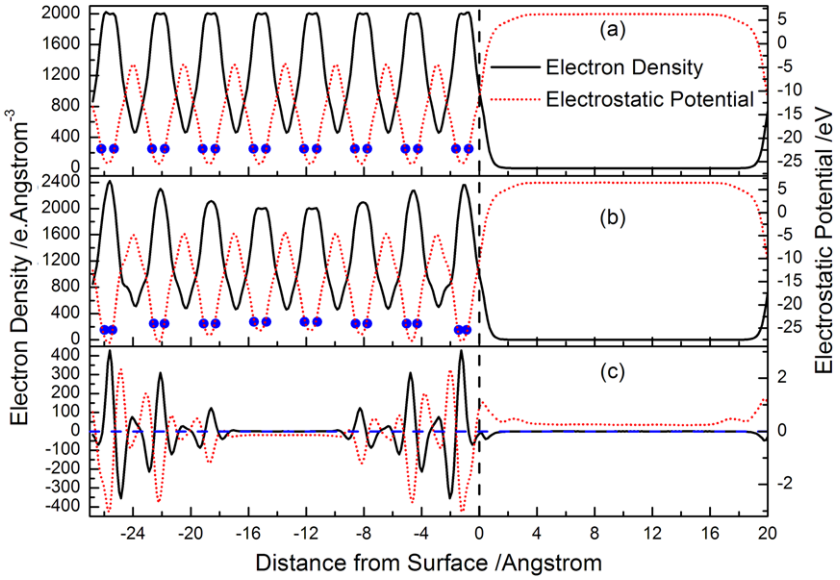

Figure 13. Electron density (black solid line) and electrostatic potential (red dotted line) of the anatase TiO_2 (101) surface. The blue solid circle denotes the position of Ti atoms. The black dashed line denotes the position of the surface, in which a positive distance means into the vacuum region and a negative distance means under the surface. The density and potential were averaged parallel to the surface and plotted as a function of distance from the surface. (a) Before surface relaxation; (b) after surface relaxation; (c) the differences of electron density or electrostatic potential.

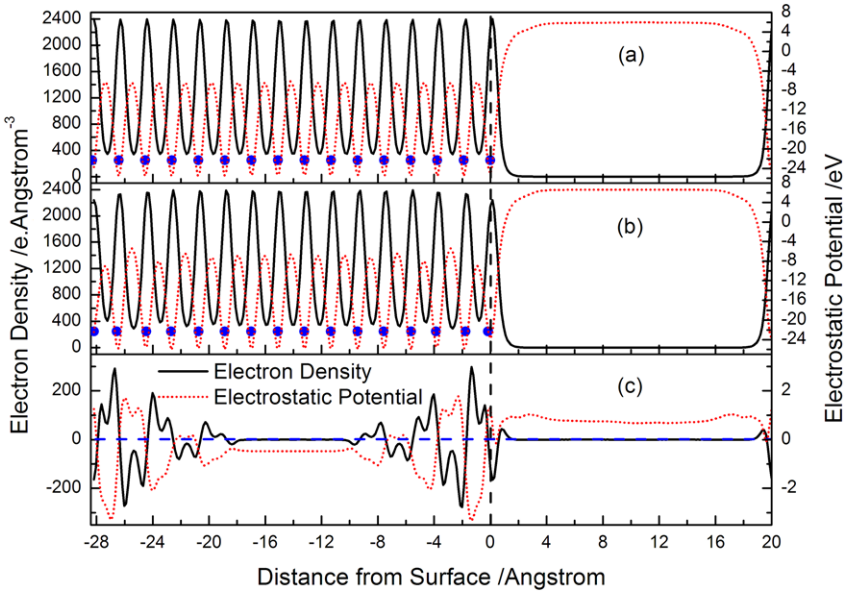

Figure 14. The same as figure 13 but for the (100) surface.

all the unrelaxed surfaces are smaller than the calculated bulk band gap. Namely, taking advantage of these surface states, one could possibly realize visible-light driven photocatalytic reactions, in which surface microstructure mediation will be used instead of impurities modification. Recently, Ariga *et al* have just reported the latest results on this aspect [59]. They found visible-light photo-oxidation of formic acid on a pure TiO_2 (001) surface.

3.3. The electronic structure (part II)

Because of the unbalanced interaction between surface atoms, the ideal surfaces will relax. Surface atomic relaxation will result in electron redistribution. In this way, the interaction between surface atoms can be balanced, and the surface achieves a stable state. Therefore, atomic relaxation and electron redistribution are closely correlated with each other. An electrostatic potential is generated by the electron distribution, so its change is directly correlated with electron redistribution. In figures 13–18, we plotted the average electron density and electrostatic potential profiles along the normal direction of surface. In order to clearly display the effect of surface relaxation, we also gave the differences for electron density or electrostatic potential before and after surface relaxation, and the positions of the titanium atoms. Based these figures, we could extract some features, as follows.

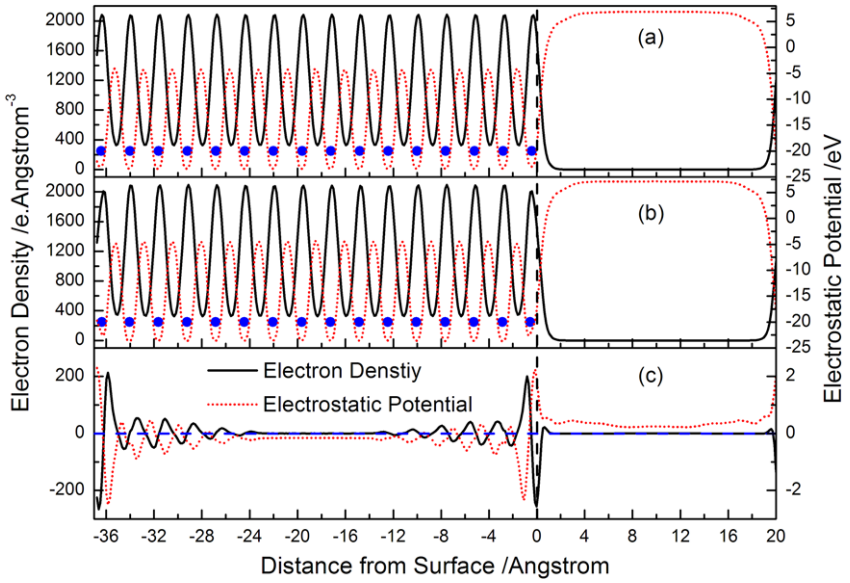

Figure 15. The same as figure 13 but for the (001) surface.

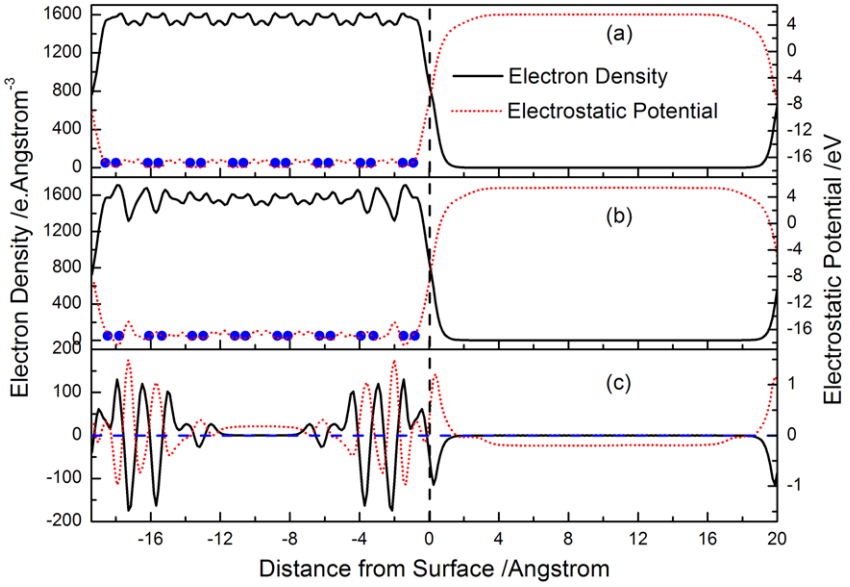

Figure 16. The same as figure 13 but for the $(103)_f$ surface.

(i) For each surface model, both the electron density and electrostatic potential already reach the same values in the vacuum region. This result indicates that the vacuum region is large enough to permit the full decay of the electron density. From the surface down, the differences tend to zero as well; this means the slab model is thick enough. So the calculated results for each surface are reliable and accurate.

(ii) For the existence of a surface, the electron densities rapidly decay to zero above the surface, while the electrostatic potential reaches a certain value in the vacuum region. This is a typical Friedel oscillation decay.

(iii) For unrelaxed surfaces, both electron density and electrostatic potential have the same periods as the lattice along the surface normal direction. This implies that the ideal surface keeps bulk features such as surface cleaving. So the work function of the unrelaxed surface reflects the electrostatic potential caused by truncating the lattice periods. As previously discussed, an atomic displacement will change the state surface dipole moment. Thus surface relaxation will induce an additional surface dipole moment, and the surface work function is changed in consequence. So we can reversely calculate the additional surface dipole moment according to the change of surface work function. These results are displayed in table 1.

(iv) At the surface position, the electron density decreases, and the electrostatic potential accordingly increases. About 1–2 Å below the surface, the difference of electron density reaches its maximum. This means that after surface

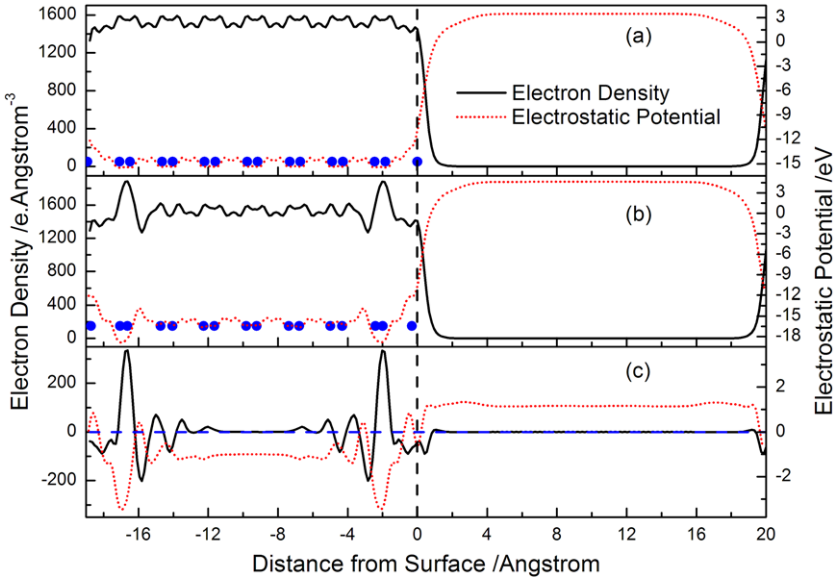

Figure 17. The same as figure 13 but for the $(103)_s$ surface.

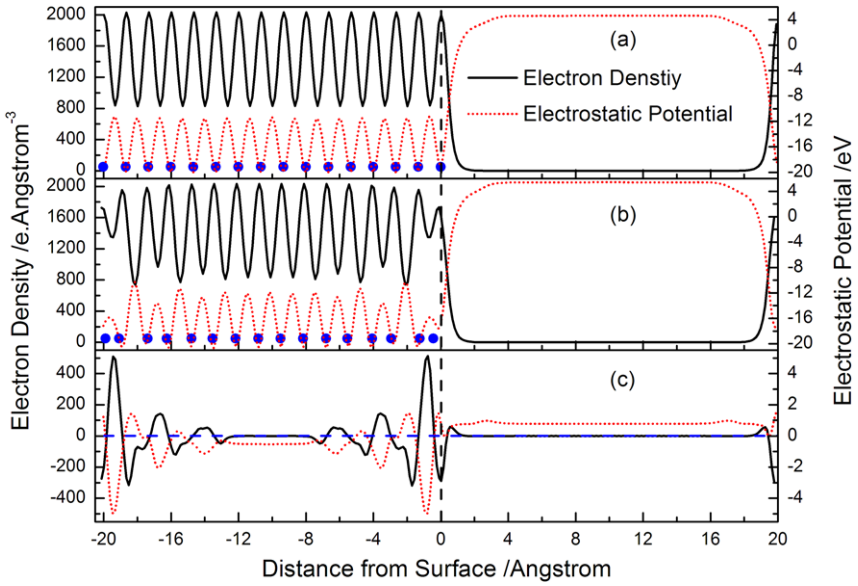

Figure 18. The same as figure 13 but for the (110) surface.

relaxation, electrons concentrate in this region. In each periodic plane, the electrons concentrate on the central oxygen atoms. As the in-depth distance increases, this trend gradually weakens.

In addition to the above common features, there are some differences in the details for different surfaces. The changes of the $(103)_f$ surface are smaller than the other surfaces. In both (103) surfaces the variations of electron density and electrostatic potential are very gentle. Except for the $(103)_f$ surface, after surface relaxation, the electrostatic potential increases in the vacuum region, while it decreases in the bulk region. In (001)/(100)/(110) surfaces, each periodic plane contains stoichiometric atoms, while in (101)/(103) surfaces, each periodic plane contains two tri-layers. The variations of electron density and electrostatic potential illustrate this point very well.

4. Summary and conclusions

As pointed out in section 3.1, after surface relaxation, anatase TiO_2 prefers to form an oxygen-rich surface. For each surface, the outermost one and/or two layers contain oxygen atoms, and their electrons transfer inward. So the outermost oxygen atoms are deficient in electrons and they tend to get electrons from adsorbate. In all the surfaces, the relaxation of (001) surface is not pronounced, and its surface energy difference is the smallest among these surfaces. On the contrary, the relaxation of the $(103)_s$ surface is very dramatic, and the

surface energy difference is the largest among these surfaces. Comparing surface energy and the change of surface dipole moment, one can see that the change of surface dipole moment is related to surface relaxation. Combined with electronic structure calculations, the more obvious surface relaxation and electron transfer the surface has, the larger additional surface dipole moment the surface has. The sequence of additional surface dipole moment is as follows: $(103)_s > (110) > (101) > (100) > (103)_f > (001)$. This type of surface dipole moment plays a significant role for anatase TiO_2 performance, especially in interacting with polar adsorbates. The work function indicates the degree of difficulty in losing electrons from the surface, while the electron affinity energy indicates the capacity for obtaining electrons from adsorbate. For anatase TiO_2 surfaces, the sequence of surface work function is as follows: $(110) < (001) < (103)_s < (100) < (103)_f < (101)$; and the sequence of surface electron affinity energy is as follows: $(103)_f > (101) > (001) > (100) > (103)_s > (110)$. Based on these results, one can understand the selective adsorption and selective activity for different anatase TiO_2 surfaces.

In the present work, the surface energy sequence is completely in accord with other theoretical results. Based on this result, some experimental results could be verified [54]. For the same reason, one could predict that anatase TiO_2 will expose not only (101) and (001) surfaces, but also (100) and (103) surfaces on the nano-scale. Combined with previous comments, one can understand that anatase TiO_2 nanoparticles have a better performance, because they have more high activity surfaces.

Overall, near the VB bottom or CB top, the surface states are localized at surface uncoordinated anions and cations, respectively. After surface relaxation, most of the surface states disappear from the band gap, and become surface resonance states. At the same time, these surface states change to extended states from localized states. Because the electrons or holes on localized states cannot freely move on the normal direction of the surface, this change is very important for TiO_2 performance. For (001) and $(103)_f$ relaxed surfaces, the surface states still remain in the fundamental band gap, so their surface band gaps are smaller than the bulk band gap.

For uncoordinated atoms that are displaced upward after surface relaxation, the energy of the surface states will be reduced; while for the uncoordinated atoms that are displaced downward after surface relaxation, the energy of surface states will be increased. For the fully coordinated atoms, the situations are just exactly the opposite. After surface relaxation, the interaction between surface atoms will be changed due to electron redistribution and bond re-hybridization. Thus the position and dispersion characteristics of the surface states will be changed. By redistribution of the surface charge and re-hybridization of the surface bonds, the interaction between surface atoms will achieve a balance, and the surface will be stabilized. Namely, redistribution of the surface charge and re-hybridization of surface bonds are the underlying reasons for surface relaxation.

In brief summary, we investigated in detail low-index stoichiometric anatase TiO_2 surfaces by means of density functional theory calculations. Firstly, we studied and compared the surface properties of different surfaces. Based on the relevant results, one can better understand the performance and crystal morphology of anatase TiO_2 nanoparticles. Secondly, we focused on the relationship between the surface relaxation and the surface electronic structure, and explored the surface relaxation mechanism. This will provide help for relevant work in controlling crystal orientation growth for special demands.

Acknowledgments

The authors acknowledge the financial support from the National Basic Research Program of China (973 Program, Grant Nos 2007CB613301 and 2007CB613305).

References

[1] Fox M A and Dulay M T 1993 *Chem. Rev.* **93** 341
[2] Kudo A and Miseki Y 2009 *Chem. Soc. Rev.* **38** 253
[3] Fujishima A and Honda K 1972 *Nature* **238** 37
[4] Fujishima A, Zhang X and Tryk D A 2008 *Surf. Sci. Rep.* **63** 515
[5] Hoffmann M R, Martin S T, Choi W and Bahnemann D W 2002 *Chem. Rev.* **95** 69
[6] Linsebigler A L, Lu G and Yates J T 2002 *Chem. Rev.* **95** 735
[7] Diebold U 2003 *Surf. Sci. Rep.* **48** 53
[8] Diebold U, Ruzycki N, Herman G S and Selloni A 2003 *Catal. Today* **85** 93
[9] Diebold U 2003 *Appl. Phys.* A **76** 681
[10] Thomas A G, Flavell W R, Mallick A K, Kumarasinghe A R, Tsoutsou D, Khan N, Chatwin C, Rayner S, Smith G C, Stockbauer R L, Warren S, Johal T K, Patel S, Holland D, Taleb A and Wiame F 2007 *Phys. Rev.* B **75** 035105
[11] Kubo T, Sayama K and Nozoye H 2006 *J. Am. Chem. Soc.* **128** 4074
[12] Vogtenhuber D, Podloucky R, Neckel A, Steinemann S G and Freeman A J 1994 *Phys. Rev.* B **49** 2099
[13] Lindsay R, Wander A, Ernst A, Montanari B, Thornton G and Harrison N M 2005 *Phys. Rev. Lett.* **94** 246102
[14] Purton J, Bullett D W, Oliver P M and Parker S C 1995 *Surf. Sci.* **336** 166
[15] Gong X Q, Khorshidi N, Stierle A, Vonk V, Ellinger C, Dosch H, Cheng H, Selloni A, He Y, Dulub O and Diebold U 2009 *Surf. Sci.* **603** 138
[16] Kubo T, Orita H and Nozoye H 2007 *J. Am. Chem. Soc.* **129** 10474
[17] Lindan P J D, Harrison N M, Gillan M J and White J A 1997 *Phys. Rev.* B **55** 15919
[18] Lindan P J D and Harrison N M 2001 *Surf. Sci.* **479** L375
[19] Bates S P, Kresse G and Gillan M J 1997 *Surf. Sci.* **385** 386
[20] Elliott S D and Bates S P 2001 *Surf. Sci.* **495** 211
[21] Hebenstreit W, Ruzycki N, Herman G S, Gao Y and Diebold U 2000 *Phys. Rev.* B **62** R16334
[22] Hengerer R, Bolliger B, Erbudak M and Gräzel M 2000 *Surf. Sci.* **460** 162
[23] Lazzeri M, Vittadini A and Selloni A 2001 *Phys. Rev.* B **63** 155409
[24] Gong X Q, Selloni A, Batzill M and Diebold U 2006 *Nat. Mater.* **5** 665
[25] Lazzeri M and Selloni A 2001 *Phys. Rev. Lett.* **87** 266105
[26] Muscat J and Harrison N M 2000 *Surf. Sci.* **446** 119
[27] Ng K-O and Vanderbilt D 1997 *Phys. Rev.* B **56** 10544
[28] Labat F, Baranek P and Adamo C 2008 *J. Chem. Theory Comput.* **4** 341

[29] Thompson T L and Yates J T 2006 *Chem. Rev.* **106** 4428
[30] Clark S J, Segall M D, Pickard C J, Hasnip P J, Probert M J, Refson K and Payne M C 2005 *Z. Kristallogr.* **220** 567
[31] Perdew J P, Burke K and Ernzerhof M 1996 *Phys. Rev. Lett.* **77** 3865
[32] Pfrommer B G, Câté M, Louie S G and Cohen M L 1997 *J. Comput. Phys.* **131** 233
[33] Burdett J K, Hughbanks T, Miller G J, Richardson J W and Smith J V 1987 *J. Am. Chem. Soc.* **109** 3639
[34] Asahi R, Taga Y, Mannstadt W and Freeman A J 2000 *Phys. Rev.* B **61** 7459
[35] Terzibaschian T and Enderlein R 1986 *Phys. Status Solidi* b **133** 443
[36] Li W X, Stampfl C and Scheffler M 2002 *Phys. Rev.* B **65** 075407
[37] Tasker P W 1979 *J. Phys. C: Solid State Phys.* **12** 4977
[38] LaFemina J P 1994 *Crit. Rev. Surf. Chem.* **3** 297
[39] Han X, Kuang Q, Jin M, Xie Z and Zheng L 2009 *J. Am. Chem. Soc.* **131** 3152
[40] Herman G S and Gao Y 2001 *Thin Solid Films* **397** 157
[41] Homann T, Bredow T and Jug K 2004 *Surf. Sci.* **555** 135
[42] Wahab H S, Bredow T and Aliwi S M 2008 *THEOCHEM-J. Mol. Struct.* **868** 101
[43] Wahab H S, Bredow T and Aliwi S M 2008 *Chem. Phys.* **353** 93
[44] Durinck G, Poelman H, Clauws P, Fiermans L, Vennik J and Dalmai G 1991 *Solid State Commun.* **80** 579
[45] Poelman H and Fiermans L 1998 *Surf. Sci. Spectra* **5** 252
[46] Ruzycki N, Herman G S, Boatner L A and Diebold U 2003 *Surf. Sci.* **529** L239
[47] Gong X Q and Selloni A 2005 *J. Phys. Chem.* B **109** 19560
[48] Yang H G, Sun C H, Qiao S Z, Zou J, Liu G, Smith S C, Cheng H M and Lu G Q 2008 *Nature* **453** 638
[49] Selloni A 2008 *Nat. Mater.* **7** 613
[50] Devriendt K, Poelman H and Fiermans L 2000 *Surf. Interface Anal.* **29** 139
[51] Gao W, Wang C M, Wang H Q, Henrich V E and Altman E I 2004 *Surf. Sci.* **559** 201
[52] Dai Y, Cobley C M, Zeng J, Sun Y and Xia Y 2009 *Nano Lett.* **9** 2455
[53] Liang Y, Gan S, Chambers S A and Altman E I 2001 *Phys. Rev.* B **63** 235402
[54] Herman G S, Sievers M R and Gao Y 2000 *Phys. Rev. Lett.* **84** 3354
[55] Gao Y and Elder S A 2000 *Mater. Lett.* **44** 228
[56] Giorgio S, Henry C R, Pauwels B and Van Tendeloo G 2001 *Mater. Sci. Eng.* A **297** 197
[57] Santra A K, Yang F and Goodman D W 2004 *Surf. Sci.* **548** 324
[58] Godby R W, Schlüter M and Sham L J 1988 *Phys. Rev.* B **37** 10159
[59] Ariga H, Taniike T, Morikawa H, Tada M, Min B K, Watanabe K, Matsumoto Y, Ikeda S, Saiki K and Iwasawa Y 2009 *J. Am. Chem. Soc.* **131** 14670